

Fermionization of Bosons in a Flat Band

Saurabh Maiti and Tigran Sedrakyan

Department of Physics, University of Massachusetts, Amherst, MA 01003

(Dated: July 1, 2019)

Strongly interacting bosons that live in a lattice with degeneracy in its lowest energy band experience frustration that can prevent the formation of a Bose-Einstein condensate. Such systems form an ideal playground to investigate spin-liquid behavior. We use the variational principle and the Chern-Simons technique of fermionization of hard-core bosons on Kagome lattice to find that below lattice filling fraction $\nu = 1/3$ the system favors a topologically ordered chiral spin-liquid state that is gapped in bulk, spontaneously breaks Time-Reversal Symmetry, and supports massless chiral bosonic edge mode. We construct the many-body variational wave function of the state and show that the corresponding energy coincides with the energy of the flat band. This result proves that the ground state of the system cannot stabilize a Bose condensate below $\nu = 1/3$. The fermionization and variational scheme we outline apply to any non-Bravais lattice. We distinguish between the roles played by the Chern-Simons gauge field in lattices with a flat band and those exhibiting a moat-like dispersion (which is degenerate along a closed contour in the reciprocal space). We also suggest experimental probes to differentiate the proposed ground state from a condensate.

I. INTRODUCTION

A quantum spin-liquid is one of the sought after states in a strongly interacting spin system. A recent neutron scattering experiment on herbertsmithite¹ reported the first detection of a spin-liquid phase. While the characterization of this state has been a matter of debate², this experiment indicates that the detection of the various spin-liquid states is not far away. Some manifestations of this state include a gapless Dirac (4-spinor) spin liquid state coupled to a U(1) gauge field^{3,4}, a gapped Z₂ spin liquid state^{2,5}, a chiral spin liquid (CSL)⁶⁻¹³ some of which can also be gapless¹⁴. Such states exhibit absence of rotational symmetry breaking and, as such, do not stabilize any long-range magnetic order. Their collective low-energy excitations support fractionalized statistics, which can be classified using topological quantum field theory with various symmetry properties. Variety of techniques have been used in the literature to identify and study the properties of such states¹⁵⁻¹⁸ with many of the early and current attempts focusing on 2D triangular and honeycomb lattices¹⁹⁻²³.

Amongst the numerous quantum spin-liquid candidates²⁴⁻²⁷, the spin-1/2 Heisenberg magnet on a Kagome lattice stands out as a fascinating system that is believed to give rise to a variety of spin-liquid phases^{28,29}. The Kagome lattice is known to possess a flat band (quenched dispersion). If the lattice is sparsely populated by strongly interacting bosons (also referred to as hard-core bosons which avoid multiple occupancy of a single site), the state of the system is determined entirely from minimization of the interactions, since the kinetic energy of the system is fully quenched. Such a system is equivalent to an XY model with the z -directional magnetic field term, $H_{mag} = \sum_{\mathbf{r}} \mu S_{\mathbf{r}}^z$. The field strength μ maps on to the chemical potential of hard-core bosons. These bosons at low densities do not condense because of the degeneracy of the condensate wave functions which arises from the flat band. In the

XY model, the absence of condensation translates to the absence of magnetic order. One is thus interested in learning about phases that can be stabilized in such a system.

It is instructive to note that if one replaces hard-core bosons by spinless fermions, the flat band would be capable of accommodating fermionic states up to $\nu = 1/3$, such that fermions avoid each other and have exactly zero energy (measured relative to the flat band) just by filling the flat band. This observation suggests that if there was a way for a system of hard-core bosons to stabilize low-energy excitations with fermionic statistics, such a state could be energetically favorable. In this article, we demonstrate the use of a technique that fermionizes hard-core bosons to find a chiral spin-liquid state as the energetically favorable candidate for the ground state of interacting spins on a Kagome lattice, which spontaneously breaks time-reversal symmetry (TRS) and represents an example where topological ordering is realized with interacting bosons.

Current understanding of the system under consideration is that the hard-core bosons can avoid paying any cost of interaction energy by forming spatially separated localized states^{30,31} which is possible due to the presence of a flat band in the Kagome lattice. Such a state can persist up to lattice filling of $\nu = 1/9$, beyond which the system is faced with a choice between (a) populating higher energy bands (see Fig. 1); and (b) letting the bosons still reside in the flat band and paying the interaction cost due to overlap. The choice (a) would result in condensation of bosons (represented by (blue) dots on E_2 in Fig. 1) to the Γ point of the Brillouin zone, leading to the supersolid state whose chemical potential grows as $\mu \sim (\nu - 1/9)$, up to logarithmic prefactors. Such a supersolid state has been predicted as a mean-field theory for weakly interacting bosons at lattice fillings above 1/9 in Ref. 31. The corresponding ground state energy E_{GS} scales as $E_{GS} \sim (\nu - 1/9)^2$.

The choice (b) essentially remains unexplored. We find

within our approach that for strongly interacting bosons in a flat band Kagome lattice the correlations lead to effective fermionization of the bosons. To this end, we show that the system can still save energy (retaining $E_{GS} \sim 0$) by continuing to populate the flat band up to $\nu = 1/3$. Interestingly enough, the scaling of the chemical potential of the fermionized system with particle density is insensitive to the filling fraction around $1/9$, which is a critical value for condensed bosons. This change in the scaling of μ with density will result in different velocity distribution curves extracted from time-of-flight experiments on trapped atoms. This suggests that such an experiment can be used as a tool to distinguish between the two possible filling states, (a) and (b), under discussion, above the $1/9$ filling.

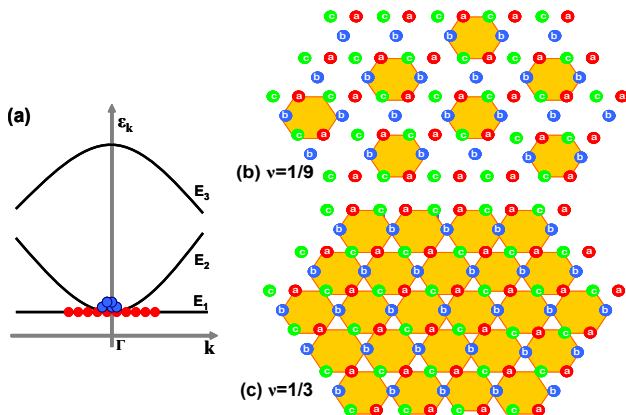


FIG. 1: (a) The electronic structure of Kagome-lattice has three bands, with the lowest band (E_1) being flat. The red and blue dots denote the population of E_1 and E_2 bands. (b) The real space depiction of the $\nu = 1/9$ state. The shaded region denotes occupancy by a boson. The wavefunctions do not overlap. (c) The real space depiction of the $\nu = 1/3$ chiral spin-liquid state obtained from fermionization.

The fermionization of hard-core bosons relies on attaching a Chern-Simons (CS) phase, $\Lambda_{\{\mathbf{r}\}}$, to a fermionic many-body wavefunction: $|\Phi_B\rangle = e^{i\Lambda_{\{\mathbf{r}\}}} |\Psi_F\rangle$ (where $\{\mathbf{r}\}$ denotes the set of coordinates of the particles, Ψ_F denotes the fermionic wavefunction, and Φ_B denotes the bosonic wavefunction). While this technique was used extensively to describe fractional quantum Hall (fQH) states³²⁻³⁵, it has also been applied to spin-orbit coupled bosons³⁶, bosons in honeycomb lattice³⁷, and bosons living on a moat³⁸. It has been shown that fermionization can stabilize topological spin ordering^{39,40}, high-temperature superconductivity⁴¹, and even a chiral spin-liquid in a moat band⁴². In the latter case, the role of magnetic frustration is mapped to the degeneracy of the lowest single-particle states of the fermions (the moat-band). In this article, we devise a scheme to fermionize bosons in a non-Bravais lattice in general which allows us to apply the fermionization technique to arbitrary lattices. For demonstration purposes, we apply our formulation to the case of Kagome lattice. We find that the trial wave-

function we propose, which by construction describes a CSL, is an eigenstate of the XY-model within a flux-smearing mean field approximation (MFA), and has the lowest many-body ground state energy. Our MFA breaks TRS and hence has non-zero flux per unit cell. The resulting spectrum has fermionic excitations and flux-flip excitations that can be understood as fractionally charged vortices with fractional self-statistics with angle $\theta = \frac{\pi}{2}$. These are semion excitations (which are examples of abelian anyons) of Kalmeyer-Laughlin CSL¹⁵. Moreover, the flat band prior to the MFA remains flat, but is now also gapped from the rest of the excited states. This provides a posteriori justification for the stability of our MFA. Indeed, using our trial wavefunction we explicitly demonstrate that the flux distribution within the unit cell is such that the flat band of the Kagome lattice is preserved upon the TRS breaking. This feature is unique to our prescription and unlike other attempts in literature to tackle a similar problem^{6,11,12}. More explicitly, we set-up a trial wavefunction in the continuum limit (although this limit is not necessary) and demonstrate that our state has the lowest energy, potentially up to $\nu = 1/3$.

It must be emphasized that the approach discussed in this article considers the effect of the CS field after the flux smearing MFA (which is consistent with the Gauss law constraint imposed by the CS terms in the original action). If one starts from the lattice gauge theory of CS field prior to the MFA^{11,12,33,43}, it is not straightforward to converge to particular flux distribution, and the question of the TRS breaking remains an interesting open question. For this work, we wish to emphasize the usefulness of our variational MFA, in light of the previous results obtained in Refs. 36,38,39,41,42, which shows that the ground state can have the lowest possible energy from small occupation numbers all the way to the one-third filling of the lattice. Importantly, our result rules out the possibility of condensation of interacting bosons [choice (a) discussed above] in the vicinity of the $\nu = 1/9$ filling fraction of the lattice. One can classify the possible CSLs based on symmetries, as done in some recent studies^{44,45}. The comprehensive classification of possible spin-liquid states based on the flux attachment procedure used in the present work is also possible, and is an open important problem that needs to be investigated in the future.

As indicated above, using fermionization technique, the CSL behavior has been suggested in systems with moats: which has a degenerate minima in the single particle spectrum. In this article we consider Kagome lattice which possess a flat band. We will discuss the differences arising in the calculation of many-body ground state energy in systems exhibiting moats and flat-bands. Finally we shall present the interesting avenues of research this approach motivates for future work.

The rest of the article is formatted as follows. Section II reviews the fermionization technique in general and presents a scheme to carry it out in a non-Bravais lat-

tice (with multiple atoms per unit cell). In Sec. III we discuss the application of the scheme to Kagome lattice and show that the CSL trial wavefunction has the lowest ground state energy. Finally in Sec. IV we summarize the work and present an outlook for the fermionization technique. An appendix is included that presents technical details of some calculations which would have cluttered the presentation in the main text.

II. FERMIONIZATION IN A NON-BRAVAIS LATTICE

Let us start by summarizing the concept of fermionization. Consider a generic N-body Hamiltonian (on a Bravais lattice) $\hat{H}(\mathbf{r}_1, \dots, \mathbf{r}_N) \equiv \hat{H}(\{\mathbf{r}\})$. Let $|\Phi_B\rangle$ be the undetermined many-body bosonic wavefunction (subject to hard-shell constraint for the particles). The many-body ground state energy, E_{GS} , for the hard-core bosons can be written as $E_{GS} = \langle \Phi_B | \hat{H}(\{\mathbf{r}\}) | \Phi_B \rangle$. The wavefunction $|\Phi_B\rangle$, describing hard core bosons can be expressed in a fermionic basis as $|\Phi_B\rangle = e^{i\Lambda_{\{\mathbf{r}\}}} |\Psi_F\rangle$, where $\Lambda_{\{\mathbf{r}\}} = \kappa \sum_{\mathbf{r}' < \mathbf{r}} \theta_{\mathbf{r}\mathbf{r}'}$ [$\theta_{\mathbf{r}\mathbf{r}'} = \arg(\mathbf{r} - \mathbf{r}')$], κ is an odd integer. Thus,

$$E_{GS} = \langle \Psi_F | e^{-i\Lambda_{\{\mathbf{r}\}}} \hat{H}(\{\mathbf{r}\}) e^{i\Lambda_{\{\mathbf{r}\}}} | \Psi_F \rangle$$

$$= \langle \Psi_F | \hat{H}(\{\mathbf{r}\}, \mathbf{A}_{\{\mathbf{r}\}}) | \Psi_F \rangle, \quad (1)$$

$$\approx \langle \Psi_c | \sum_{\{\mathbf{r}\}} \hat{H}^{MFA}(\mathbf{r}, \mathbf{A}_{\mathbf{r}}) | \Psi_c \rangle. \quad (2)$$

Here the non local vector potential $\mathbf{A}_{\{\mathbf{r}\}} \equiv \partial_{\mathbf{r}} \Lambda_{\{\mathbf{r}\}}$ enters into the Hamiltonian via covariant derivative $-i\partial_{\mathbf{r}} \rightarrow -i\partial_{\mathbf{r}} + \mathbf{A}_{\{\mathbf{r}\}}$. This amounts to a magnetic field of $\mathbf{B}(\mathbf{r}) \equiv \nabla \times \mathbf{A}_{\{\mathbf{r}\}} = \sum_i 2\pi\kappa\delta(\mathbf{r} - \mathbf{r}_i)$. While, the wavefunction $|\Psi_F\rangle$ in Eq. (1) is still undetermined, Eq (2) presents a way to estimate E_{GS} and needs further explanation. To go from $\hat{H}(\{\mathbf{r}\}, \mathbf{A}_{\{\mathbf{r}\}})$ to $\hat{H}^{MFA}(\mathbf{r}, \mathbf{A}_{\mathbf{r}})$, we perform a flux-smearing MFA. The essence of this approximation is that $\mathbf{B}(\mathbf{r}) = \sum_i 2\pi\kappa\delta(\mathbf{r} - \mathbf{r}_i) \rightarrow 2\pi\kappa\langle \hat{n}(\mathbf{r}) \rangle = 2\pi\kappa\nu$. That is, the field that was pinned to every particle, is smeared and treated as uniform. This MFA is consistent with the Gauss law constraint ($B = 2\pi\kappa\nu$) imposed by the CS field prior to performing the MFA.

An important distinction is to be made here. In the continuum limit, at large enough length scales such that $|\mathbf{r}| \sim l \gg 1/\sqrt{\text{density}}$, the Gauss law constraint can be accounted for by introducing a local $\mathbf{A}_{\mathbf{r}}$ such that $\nabla \times \mathbf{A}_{\mathbf{r}} = \mathbf{B}$. For the lattice version of this approximation, we require the constraint to be implemented at the level of ‘flux per unit cell’ (hence B is related directly to ν in the above formulas and not the density). For the case of 1 atom per unit cell with nearest neighbor hoppings, the flux configuration of the CS field is no different from the usual Maxwell field. The wavefunctions $|\Psi_c\rangle$ in Eq. (2) is then formed from the Slater determinant of the single particle states of $\hat{H}(\mathbf{r}, \mathbf{A}_{\mathbf{r}})$.

For a non-Bravais lattice, neither the nature of flux smearing MFA, nor the construction of a variational

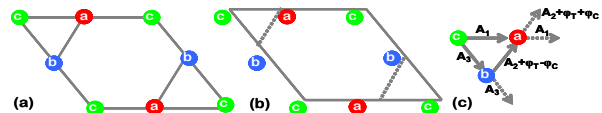


FIG. 2: (a) A unit cell of the Kagome lattice. (b) The unit cell redrawn with a shift. This explicitly shows that the cell area includes 3 atoms. The dashed lines are the internal bonds chosen to not include any atoms in the triangular loop. All the particles, and hence the flux, is contained within the hexagon. (c) Flux attachment within the unit cell of the Kagome lattice. A_i denotes the phase accumulated by $\mathbf{A}(\mathbf{r})$ while traversing the direction \mathbf{a}_i such that $A_1 = A_2 + A_3$.

many-body state is straightforward. When there are two (or more) atoms per unit cell, had we carried out the flux smearing approximation as for a Bravais lattice, there would be no distinction between the Maxwell-type field and CS field. We realize that small enough length scales $|\mathbf{r}| \sim \text{lattice constant}$, the flux distribution within a unit cell must depend on the relative locations of atoms within the unit cell. Thus it is possible to implement the Gauss-law constraint at the level of unit cell and still be left with a degree of freedom in distributing the flux internally in the unit cell. To implement this feature, we propose that this can be implemented by requiring that all the hops that form loops internal to the unit cell (not more than one sharing edge), must not enclose any flux. This is based on the observation that in the absence of CDW ordering, the homogeneous CS flux attachment preserves the fact that if there is a triangle composed of two nearest-neighboring and one next-nearest-neighboring sites, then there must be such triangle within the unit cell where two subsequent hops along the links of nearest-neighboring sites are equivalent to a single hop along the next-nearest-neighbor link, see approaches in Refs. 36,38,39,42,46.

Note that if we have only one atom per unit cell (Bravais lattice), then there are no internal loops possible and thus the CS flux is the same as Maxwell flux. However, when we consider a non-Bravais lattice which contains loops of hops internal to the unit cell, there can be parts of the unit cell with zero net flux^{37,38}. This is seen by redrawing the unit cell as in Fig. 2b. The flux smearing field that confirms with the Gauss law can be accounted for by $\mathbf{A}_{\mathbf{r}}$ which introduces a flux ϕ_T per triangular region of the Kagome lattice. To account for the zero flux regions, one must introduce an intra-unit cell flux $\phi_C = \phi_T$ as in Figs. 2c,3. This introduction is lattice dependent and will be demonstrated later for the Kagome lattice.

Having demonstrated the non-triviality in the flux smearing MFA, we now address the subtlety in constructing the many-body wavefunction. The Hamiltonian matrix in a non-Bravais lattice has a rank, n , that is the number of atoms in the basis of the lattice. An N -body wavefunction can be denoted as $\Psi_{\{n\}}^{\{a\}}(\{\mathbf{r}\}) \equiv \Psi_{n_1, n_2, \dots, n_N}^{a_1, a_2, \dots, a_N}(\mathbf{r}_1, \mathbf{r}_2, \dots, \mathbf{r}_N)$, where a given coordinate \mathbf{r}_i can describe the wavefunction component

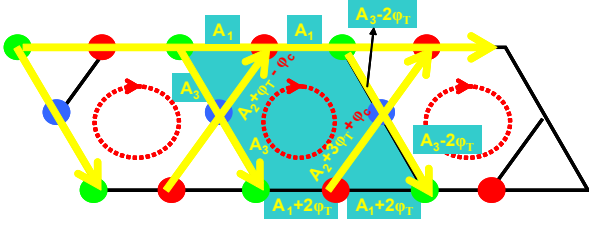


FIG. 3: Extended scheme for the flux attachment. Note that ϕ_T grows to account for the area law, where as ϕ_C is the same in every unit cell. The flux through the hexagon and the unit cell is $8\phi_T$ and through any triangle is $\phi_T - \phi_C$. In our MFA $\phi_T = \phi_C$.

$a_i \in \{1, 2, \dots, n\}$ in quantum state n_i . Correspondingly, the N-body Hamiltonian acquires the form $\hat{H}_{\{ab\}}(\{\mathbf{r}\}) \equiv$

$$\hat{H}_{a_1 b_1, \dots, a_N b_N}(\mathbf{r}_1, \dots, \mathbf{r}_N) = \sum_{i=1}^N \hat{H}_{a_i b_i}(\mathbf{r}_i) \prod_{j \neq i}^N \delta_{a_j b_j}. \quad (3)$$

The presence of a basis in a non-Bravais lattice introduces a degree of freedom in implementing the antisymmetrization: if the single particle states are given by $\psi_n^a(\mathbf{r})$, where n denotes the band and a denotes the component of the wavefunction, the most general construction of a fermionic N-body state is

$$\Psi_{\{s\}}(\{\mathbf{r}\}) = M_{\{s\}}^{s_1 s_2 \dots s_N} \times \frac{1}{\sqrt{N!}} \text{Det} [\psi_{n_1, n_2, \dots, n_N}^{s_1, s_2, \dots, s_N}(\mathbf{r}_1, \mathbf{r}_2, \dots, \mathbf{r}_N)], \quad (4)$$

where $s, s_i \in \{1, 2, \dots, N\}$, the repeated indices are summed over, and the Slater determinant is formed out of the indices n_i and \mathbf{r}_i . The tensor M superposes the anti-symmetrized Slater determinants for various combinations of $\{s_i\}$. The constraints on M are enforced by requiring the many-body wavefunction be normalized to unity, and that the permutation properties of M must respect antisymmetrization. This formally sets up a variational problem where the choice of the M -tensor is variational. The problem of such a huge variational space can be overcome by resorting to another technique to guess a trial wave-function, which we discuss next.

A. Trial wavefunction by projection to a band

We note that a single particle state is indexed as $\psi_{n, \mathbf{k}}^a(\mathbf{r})$. Indices a and n are necessary to account for the non-Bravais nature of the lattice. Index \mathbf{k} reflects the crystal translational symmetry which is independent of the non-Bravais nature and allows us to write (see Appendix C)

$$\psi_{n, \mathbf{k}}^a(\mathbf{r}) = \int_{\mathbf{r}'} R_n^a(\mathbf{r} - \mathbf{r}') \phi_{\mathbf{k}}(\mathbf{r}'), \quad (5)$$

where $\phi_{\mathbf{k}}(\mathbf{r})$ is a solution to the characteristic equation of $\hat{H}_{ab}(\mathbf{r})$, and $R_n^a(\mathbf{r})$ is the Fourier transform of the eigenvectors of $H_{ab}(\mathbf{k})$. The normalization condition is enforced by requiring $\int_{\mathbf{r}_1, \mathbf{r}_2, \mathbf{r}} \sum_a \phi_{\mathbf{k}}^*(\mathbf{r}_2) R_n^{a*}(\mathbf{r} - \mathbf{r}_1) R_n^a(\mathbf{r} - \mathbf{r}_2) \phi_{\mathbf{k}}(\mathbf{r}_2) = 1$. The many-body wavefunction can then be constructed as

$$\Psi_{\{n, \mathbf{k}\}}^{\{a\}}(\{\mathbf{r}\}) = \int_{\{\mathbf{r}'\}} R_{n_1}^{a_1}(\mathbf{r}_1 - \mathbf{r}'_1) \dots R_{n_N}^{a_N}(\mathbf{r}_N - \mathbf{r}'_N) \phi_{\{\mathbf{k}\}}(\{\mathbf{r}'\}). \quad (6)$$

Here $\phi_{\{\mathbf{k}\}}(\{\mathbf{r}\})$ denotes the N-body wavefunction formed out of the quantum states $\{\mathbf{k}\}$ and coordinates $\{\mathbf{r}\}$. The energy expectation value of band n and quantum states $\{\mathbf{k}\}$ is given by

$$E_n(\{\mathbf{k}\}) = \sum_{\{a\}, \{b\}} \int_{\{\mathbf{r}\}} \Psi_{\{n, \mathbf{k}\}}^{\{a\}*}(\{\mathbf{r}\}) \hat{H}_{\{ab\}}(\{\mathbf{r}\}) \Psi_{\{n, \mathbf{k}\}}^{\{b\}}(\{\mathbf{r}\}). \quad (7)$$

Using Eq. (3), together with the normalization condition, we can show that

$$E_n(\{\mathbf{k}\}) = \int_{\{\mathbf{r}'\} \{\mathbf{r}''\}} \phi_{\{\mathbf{k}\}}^*(\{\mathbf{r}'\}) E_n(\{\mathbf{r}'\}, \{\mathbf{r}''\}) \phi_{\{\mathbf{k}\}}(\{\mathbf{r}''\}), \quad (8)$$

where we introduced a notation

$$E_n(\{\mathbf{r}'\}, \{\mathbf{r}''\}) = \sum_{\{a\} \{b\}} \int_{\{\mathbf{r}\}} \prod_i R_n^{a_i}(\mathbf{r}'_i - \mathbf{r}_i) \times \hat{H}_{\{ab\}}(\{\mathbf{r}\}) \prod_j R_n^{b_j}(\mathbf{r}_j - \mathbf{r}''_j). \quad (9)$$

We have thus devised a way to remove the index dependence of $\hat{H}_{ab}(\mathbf{r})$ and map it to a single component energy function $E_n(\mathbf{r}', \mathbf{r}'')$ with single component wavefunction $\phi_{\mathbf{k}}(\mathbf{r})$. The advantage of doing this is that we can readily use Eqs (1) and (2) without resorting to multicomponent nature of H , which may lead to introduction of a non-Abelian CS field. The many body state $\phi_{\{\mathbf{k}\}}(\{\mathbf{r}\})$ has to be bosonic. But it can be fermionized as:

$$\phi_{\{\mathbf{k}\}}(\{\mathbf{r}\}) = e^{i\Lambda_{\{\mathbf{r}\}}} \psi_{\{\mathbf{k}\}}(\{\mathbf{r}\}), \quad (10)$$

where $\psi_{\{\mathbf{k}\}}(\{\mathbf{r}\})$ is a Slater determinant. Thus the fermionized version of Eq. (8) can be achieved by promoting

$$\begin{aligned} \phi_{\{\mathbf{k}\}}(\{\mathbf{r}\}) &\rightarrow \psi_{\{\mathbf{k}\}}(\{\mathbf{r}\}), \text{ and} \\ E_n(\{\mathbf{r}'\}, \{\mathbf{r}''\}) &\rightarrow e^{-i\Lambda_{\{\mathbf{r}'\}}} E_n(\{\mathbf{r}'\}, \{\mathbf{r}''\}) e^{i\Lambda_{\{\mathbf{r}''\}}}. \end{aligned} \quad (11)$$

We note that while $\hat{H}(\{\mathbf{r}\})$ is entirely the property of the underlying lattice, the construction of E_n and the choice of ψ is a variational knob available to us. Thus we have traded the M-tensor based variational space with the choice of $E_n(\mathbf{r}, \mathbf{r}')$. In what follows, we demonstrate that a trial wavefunction for hard-core bosons on Kagome lattice, derived from the above scheme, describes a CSL with spontaneously broken TRS and has the lowest possible E_{GS} .

III. KAGOME LATTICE AND THE MANY-BODY TRIAL WAVEFUNCTION

In general, the problem of hard core bosons on a lattice can be studied by looking at the spin-1/2 XY model with Hamiltonian

$$H = \sum_m J_m \sum_{\mathbf{r},n} S_{\mathbf{r}}^+ S_{\mathbf{r}+\mathbf{r}_{mn}}^- + \text{h.c.} \quad (12)$$

Here $S^{\pm} = S_x \pm iS_y$ are the spin-1/2 operators; the index n scans all the neighbors at distance m ; $\mathbf{r}_{m,n}$ is the vector to the $(m,n)^{\text{th}}$ nearest neighbor. The choice of lattice is reflected in the choice various \mathbf{r}_{mn} . One choice of the phase attachment (in second-quantized notation) that accomplishes the CS transformation is³²⁻³⁴

$$S_{\mathbf{r}}^+ = c_{\mathbf{r}}^{\dagger} e^{i\Lambda_{\mathbf{r}}}, \quad S_{\mathbf{r}}^- = e^{-i\Lambda_{\mathbf{r}}} c_{\mathbf{r}}, \quad (13)$$

where $c_{\mathbf{r}}^{\dagger}$ is a fermionic creation operator, and

$$\Lambda_{\mathbf{r}} \equiv \kappa \sum_{\mathbf{r}' \neq \mathbf{r}} \theta_{\mathbf{r}\mathbf{r}'} c_{\mathbf{r}'}^{\dagger} c_{\mathbf{r}}. \quad (14)$$

This transforms the Hamiltonian to a fermionic basis:

$$H = \sum_m J_m \sum_{\mathbf{r},n} c_{\mathbf{r}}^{\dagger} e^{i\Lambda_{\mathbf{r},\mathbf{r}+\mathbf{r}_{mn}}} c_{\mathbf{r}+\mathbf{r}_{mn}} + \text{h.c.}, \quad (15)$$

where $\Lambda_{\mathbf{r}_1,\mathbf{r}_2} \equiv \Lambda_{\mathbf{r}_1} - \Lambda_{\mathbf{r}_2}$ evaluated along the line joining \mathbf{r}_1 and \mathbf{r}_2 . It is the analog of the accumulated phase $\int_{\mathbf{r}_1}^{\mathbf{r}_2} \mathbf{A} \cdot d\mathbf{l}$ in a lattice. Geometrically, $\Lambda_{\mathbf{r}_1,\mathbf{r}_2}$ is the sum of the angles subtended by the vector $\mathbf{r}_1 - \mathbf{r}_2$ at every other site (located at \mathbf{r}'), weighted by the occupation probability of all sites along the path $\mathbf{r}_1 \rightarrow \mathbf{r}_2$.

From here on we specialize to the Kagome lattice with the first neighbor hoppings. This is achieved by setting $m = 1$, and letting n scan from 1 through 4 (4 nearest neighbors) for each of the three atoms in the unit cell. The MFA leads to $c_{\mathbf{r}}^{\dagger} c_{\mathbf{r}} \rightarrow \langle c_{\mathbf{r}}^{\dagger} c_{\mathbf{r}} \rangle = n_{\mathbf{r}} = \nu$ (the filling fraction in the lattice) in the definition of $\Lambda_{\mathbf{r}}$. Let the lattice now be populated by hard-core bosons at every site with filling fraction ν . Within our MFA, this provides non-zero flux at each site, spontaneously breaking TRS. The flux distribution is such that all the flux ($3 \times 2\pi\nu\kappa$) is concentrated through the hexagon (Fig 3). To achieve this, one has to introduce two fluxes ϕ_T [to account for the Maxwellian field $\mathbf{A}_{\mathbf{r}}$], and ϕ_C (to account for the the intra unit cell flux modulation). In the absence of any external field, the CS field requires $\phi_C = \phi_T = 3\pi\nu\kappa/4$.

We take note of the fact that the single particle ‘Hofstadter’ spectrum of this system is sensitive to the flux distribution within the unit cell. Figure 4a,b demonstrates that different flux distributions lead to different spectra. The property of the CS flux distribution seems to be that (i) the spectrum is unique up to $\nu = 1/3$ at which point the flux through the unit cell is 2π ; (ii) the lowest energy band is still flat! We thus observe that a CS-flux distribution in the Kagome unit cell leads to an isolated flat band.

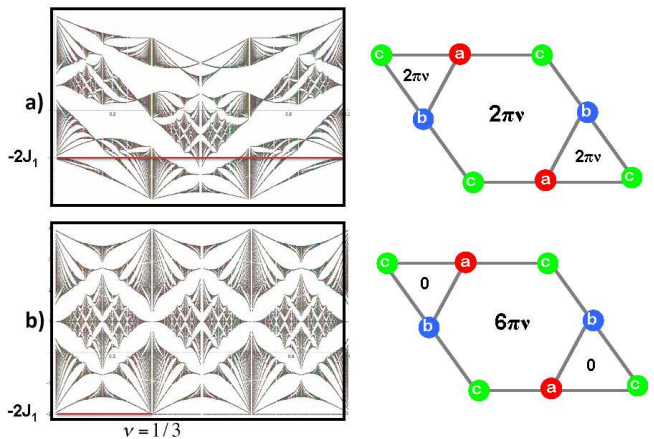


FIG. 4: Comparison of the Kagome energy spectrum in a CS field for two different flux distributions (a) and (b). The flat band is preserved in (b) where the flux through the triangle is zero. In this case, the spectrum is unique only up to $\nu = 1/3$.

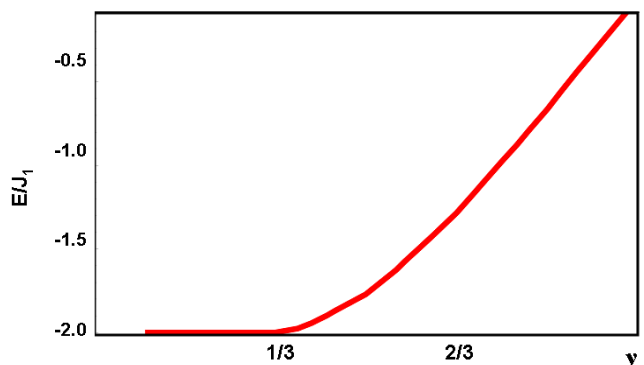


FIG. 5: Ground state energy of non-interacting fermions in Kagome lattice subject to the CS flux at mean-field level. Energy begins to rise after $\nu = 1/3$ filling.

We now resort to calculating E_{GS} where we will need the many-body trial wavefunction. To be explicit, we shall demonstrate this in the continuum limit. We iterate that to calculate E_{GS} for the original Hamiltonian, we make an estimate using a trial wavefunction which is bosonic, but constructed out of a (fermionic) slater determinant by attaching a CS phase. The single particle states needed to construct this slater determinant are the eigenstates of the Hamiltonian obtained after the flux-smearing approximation. Further, since the original Hamiltonian has three bands, we focus of forming the slater determinant from the single particle states of the band in which the chemical potential is expected to lie. Since we will be addressing the low-density regime, we expect the chemical potential to lie in the lowest band. Using the projection technique introduced above, we can express E_{GS} in terms of $E_n(\mathbf{r},\mathbf{r}')$, where n corresponds to the lowest flat band [see Eqs. (8)-(11)].

We choose R_n^a and ψ to be the eigenstates of the

$\hat{H}^{\text{MFA}}(\mathbf{r}, \mathbf{A}_\mathbf{r})$. This estimate for E_{GS} is expected to account for the non-local nature of $\mathbf{A}(\{\mathbf{r}\})$ and provide corrections to the many-body energy computed within MFA (Fig. 5). We shall explicitly demonstrate this in the continuum limit where the Hamiltonian in Eq. (12) after flux smearing can be written as:

$$\hat{H}^{\text{MFA}}(\mathbf{r}) = J_1 \begin{pmatrix} 0 & H_2 & H_1 \\ H_2^* & 0 & H_3 \\ H_1^* & H_3^* & 0 \end{pmatrix}, \quad (16)$$

where $H_i \equiv (e^{i\mathbf{p}\cdot\mathbf{a}_i/2} + e^{-i\mathbf{p}\cdot\mathbf{a}_i/2})$, $i \in \{1, 3\}$; $H_2 \equiv (e^{i\mathbf{p}\cdot\mathbf{a}_2/2} + e^{-i\mathbf{p}\cdot\mathbf{a}_2/2}) e^{i\phi_C}$; $\mathbf{p} \equiv -i\partial_\mathbf{r} + \mathbf{A}_\mathbf{r}$, $p_i \equiv \mathbf{a}_i \cdot \mathbf{p}$; and $\mathbf{a}_1 = a(1, 0)$; $\mathbf{a}_2 = a(1, \sqrt{3})/2$; $\mathbf{a}_3 = \mathbf{a}_1 - \mathbf{a}_2$ are the translation vectors. It is understood that the Hamiltonian is to be expanded to $\mathcal{O}(p^2)$. The resulting characteristic equation is

$$\frac{E}{J_1} \left(\frac{E}{J_1} + 2 \right) \left[\left(\frac{E}{J_1} + 2 \right) \left(\frac{E}{J_1} - 4 \right) + \frac{3}{2} \mathbf{p}^2 \right] \psi(\mathbf{r}) = 0. \quad (17)$$

It can be shown that $E = 0$ is a trivial solution. The eigenvalues are thus $E_1 = -2J_1$, $E_{2/3} = J_1 \left(1 \mp \sqrt{9 - 3Ba^2(m+1/2)} \right)$, $m \in \{0, 1, 2, \dots\}$, and $\mathbf{B} = \nabla \times \mathbf{A}_\mathbf{r}$. Note that the flat band E_1 is gapped from the rest of the dispersing bands ($E_{2,3}$) by $3J_1(1 - \sqrt{1 - Ba^2/6})$. From Eq. (16), we note that the wavefunction components $\psi^i \equiv \int R^i \psi$ ($i \in a, b, c$) for E_1 satisfy

$$\begin{aligned} [-p_2^2] \psi^a + [p_2 p_3 - i(\phi_T - \phi_C)] \psi^c &= 0, \\ [p_3 p_2 + i(\phi_T - \phi_C)] \psi^a + [-p_3^2] \psi^c &= 0, \end{aligned} \quad (18)$$

where $\phi_T \equiv \frac{\sqrt{3}}{16} Ba^2$ (measured counterclockwise). In the absence of any external magnetic field, the CS flux constraint requires $\phi_T = \phi_C$. Up to $\mathcal{O}(p^2)$, we can also show that the wavefunction corresponding to E_1 and in quantum state i is (see Appendix D) for calculation of \mathcal{N}):

$$\psi_i(\mathbf{r}) = \frac{1}{\mathcal{N}} \begin{pmatrix} p_3 \\ -p_1 \\ p_2 \end{pmatrix} f_i(\mathbf{r}), \quad (19)$$

where \mathcal{N} is a normalization constant and $f_i(\mathbf{r})$ can be any function that decays stronger than $1/r^2$ (for normalizability). Similar to the Landau problem for free electrons, flat band wavefunctions in the presence of CS field are also inherently localized. To impose analyticity of the wavefunction, we postulate $f_i(\mathbf{r}) = e^{-(\mathbf{r}-\mathbf{R}_i)^2/2l_{CS}^2}$, where \mathbf{R}_i is the center of the localized state, and l_{CS} is an undermined localization length scale in the theory.

A. Ground-state energy beyond single particle spectrum

The energy profile with respect to the filling fraction at the single particle level is provided in Fig. 5. Having

found the wavefunction of a gapped isolated flat band, we can use Eqs. (8)-(11) with $n = 1$ for low enough density. We observe that because of the non-dispersing nature of the isolated flat band, the effect of the non-local $A_{\{\mathbf{r}\}}$ drops out and the many-body ground state energy is still the same ($E_{GS} = -2J_1$) as computed within the single particle picture. In other words, there is no statistical correction to the E_{GS} estimated from the single particle spectrum. This is, however, only true up to $\nu = 1/3\kappa$. This is special case of flat bands and is not true for other cases of fermionization³⁶, e.g. when there is a moat band. In the case of a moat, the statistical correction to E_{GS} from the flux attachment procedure leads to a scaling³⁶ $E_{GS} \sim \mu^2 \ln^2 \mu$ which is still lower than other proposals for the corresponding ground state without Fermionization.

The reason for the statistical correction to exist for the moat and not for the flat band can be attributed to the fact that a moat is degenerate along a 1-D manifold. This means that any finite μ requires populating energy levels away from the moat levels (which have the minimum energy). In an isolated flat band, this scenario does not arise. Residual interactions between bosons (or the corresponding fermions) will lead to energy corrections but the details depend on modeling the interaction matrix element and is beyond the scope of this work.

Returning back to the lattice problem, we may ask up to what filling does the statistical correction remain zero? This can be answered by noting that attaching a flux of p/q to a unit cell causes the BZ to fold over q -times. We have proven that a CS flux distribution ($p \neq 0$) retains the flat band of the system at $p = 0$. A remarkable consequence of this is that for any q the degeneracy of the flat band is always the same as the system with no flux attachment. This can only be split by residual interactions. For a Kagome lattice with N unit cells ($3N$ atoms), N states correspond to the flat band. Even though the flux attachment changes with ν , we can now conclude that the flat band can remain occupied up to $\nu = 1/3$ (for $\kappa = 1$). This state is depicted in Fig. 1c. Thus we can rigorously state that the statistical correction is absent up to $\nu = 1/3$.

In the absence of residual interactions, the contribution to the many-body ground state only comes from the lowest energy of the single particle spectrum. Since we have demonstrated that, up to $\nu = 1/3$ (for $\kappa = 1$), the statistical correction (which has to be positive definite) is zero, this has to be the minimum energy ground state.

We take note of the fact that the spinless fermionic description, where no spatial symmetry is broken, naturally implies lack of any spin-ordering in the language of hard-core bosons. Thus, fermionization is a natural tool that can be used to describe a spin-liquid state in strongly interacting bosons. Since our MFA breaks TRS, we expect the spin-liquid state to be chiral. At this stage, we are able to conclude that strongly interacting bosons in a Kagome lattice favor a chiral spin-liquid state that spontaneously breaks TRS.

Further, the flux modulation in Figs.3 and 4b actually corresponds to a Chern insulator with staggered flux $\phi_C = 3\pi\kappa/4$ threading corner equilateral triangles of the unit cell with $-2\phi_C$ threading the hexagon, superposed with a uniform external flux of $8\phi_T = 6\pi\nu\kappa$ per unit cell. Any finite ϕ_C opens a gap at the band-touching points and defines Chern numbers for each of the three bands. The lowest band, in this case, will have a Chern number $C = 1$, which cannot be altered unless the system undergoes a phase transition with the closing of the gap. Thus the field theory of chiral spin-liquid outlined above can be regarded as a theory topologically nontrivial Chern insulator coupled to the fluctuating Chern-Simons gauge field. Because of the topological nature of the Chern insulator, Fermion fluctuations here will give rise to an additional Chern-Simons term in the low-energy effective action giving a Chern-Simons theory defined by a “K matrix” with $K = 2$ ⁴⁷. This implies that the vortex excitations in this system have fractional statistics⁴⁸ with statistical angle $\theta = \pi/2$ corresponding to semions.

IV. SUMMARY AND OUTLOOK

We prescribed a general scheme to construct the N-body wavefunction and compute the ground state energy of hard-core bosons in a non-Bravais lattice using fermionization. Using the example of the Kagome lattice, we showed that a CS type flux attachment can retain the massive degeneracy of system’s original electronic structure. Our trial wavefunction suggests that the ground state of hard-core bosons on a Kagome lattice is a spontaneously TRS broken chiral spin-liquid state. We proved that our trial wavefunction has zero statistical correction to the ground state energy due to a 2-dimensional degeneracy of the flat band in a Kagome lattice. It is thus a lowest energy state that implies absence of condensation of hard core bosons below third-filling (including the vicinity of the $\nu = 1/9$ lattice filling fraction discussed above). While within our analysis, it is not possible to determine the uniqueness of this spin-liquid ground state, corroboration with other numerical techniques (e.g. DMRG) can help confirm this state.

The lattice itself can be realized using a cold atom set-up as in Ref. 49. In this reference, to ensure that the flat band is the lowest of the three, one can tune the lattice to the frustrated hopping regime with the help of artificial gauge fields attaching π phases to all links resulting in the flipped sign of the matrix element. Other verifiable properties are bosonic edge states (can be detected using sudden decoupling technique⁵⁰); and fractional excitations (time-of-flight experiments and Bragg spectroscopy^{51–53}).

Acknowledgements: We are grateful to A. Kamenev and L. I. Glazman for useful discussions. T.A.S. thanks the Aspen Center for Physics (supported by National Science Foundation grant PHY-1607611) and the Max

Planck Institute for the Physics of Complex Systems for hospitality. The work is supported by startup funds from UMass Amherst.

Appendix A: Momentum space to real space wavefunctions

Prior to implementing the MFA, we quickly review the Kagome Hamiltonian at the single particle level and find the wavefunctions of the flat band in the continuum limit. This will set us up to tackle the scenario with the CS flux distribution. The lattice Hamiltonian from Eq. (15), without Λ can be written in \mathbf{k} -space as

$$H = \sum_{\mathbf{k}} \bar{\Psi}_{\mathbf{k}}^\dagger \bar{\mathcal{H}}_{\mathbf{k}} \bar{\Psi}_{\mathbf{k}}, \quad (\text{A1})$$

where $\bar{\Psi}_{\mathbf{k}}^\dagger = (\bar{c}_{a,\mathbf{k}}^\dagger, \bar{c}_{b,\mathbf{k}}^\dagger, \bar{c}_{c,\mathbf{k}}^\dagger)$. The annihilation operators are given by

$$\bar{c}_{x,\mathbf{r}} = \sum_{\mathbf{k}} \bar{c}_{x,\mathbf{k}} e^{i\mathbf{k}\cdot\mathbf{r}},$$

such that $x \in \{a, b, c\}$. The vector \mathbf{r} only runs over lattice translations and not internal bonds. Lastly,

$$\bar{\mathcal{H}}_{\mathbf{k}} = J_1 \begin{pmatrix} 0 & (1 + e^{i\mathbf{k}\cdot\mathbf{a}_2}) & (1 + e^{i\mathbf{k}\cdot\mathbf{a}_1}) \\ (1 + e^{-i\mathbf{k}\cdot\mathbf{a}_2}) & 0 & (1 + e^{i\mathbf{k}\cdot\mathbf{a}_3}) \\ (1 + e^{-i\mathbf{k}\cdot\mathbf{a}_1}) & (1 + e^{-i\mathbf{k}\cdot\mathbf{a}_3}) & 0 \end{pmatrix}, \quad (\text{A2})$$

where

$$\mathbf{a}_1 = a(1, 0); \quad \mathbf{a}_2 = a \left(\frac{1}{2}, \frac{\sqrt{3}}{2} \right); \quad \mathbf{a}_3 = a \left(\frac{1}{2}, -\frac{\sqrt{3}}{2} \right).$$

Note that in addition to the lattice translation vectors \mathbf{a}_1 and \mathbf{a}_2 , we have introduced $\mathbf{a}_3 = \mathbf{a}_1 - \mathbf{a}_2$. It will be useful to perform a gauge transformation: $\mathcal{H}_{\mathbf{k}} = M^\dagger \bar{\mathcal{H}}_{\mathbf{k}} M$ and $\Psi_{\mathbf{k}} = M^\dagger \bar{\Psi}_{\mathbf{k}}$ where $M^\dagger = \text{diag}(1, e^{-i\mathbf{k}\cdot\mathbf{a}_2/2}, e^{-i\mathbf{k}\cdot\mathbf{a}_1/2})$ such that

$$\mathcal{H}_{\mathbf{k}} = J_1 \begin{pmatrix} 0 & H_2 & H_1 \\ H_2 & 0 & H_3 \\ H_1 & H_3 & 0 \end{pmatrix}, \quad (\text{A3})$$

and $H_i \equiv (e^{i\mathbf{k}\cdot\mathbf{a}_i/2} + e^{-i\mathbf{k}\cdot\mathbf{a}_i/2})$. The resulting characteristic equation to find the eigenvalues is

$$\left(\frac{E}{J_1} \right)^3 - \frac{E}{J_1} (H_1^2 + H_2^2 + H_3^2) - 2H_1 H_2 H_3 = 0. \quad (\text{A4})$$

The eigenvalues are $E_1 = -2J_1$ and $E_{2/3} = J_1 (-1 \mp \sqrt{1 + H_1 H_2 H_3})$. Note that E_1 is independent of any parameters in the Hamiltonian and hence dispersionless. The wavefunction corresponding to this flat band is

$$\Psi_{\mathbf{k}}^1 = \frac{1}{N_1} \begin{pmatrix} e^{i(\mathbf{k}\cdot\mathbf{a}_1 + \mathbf{k}\cdot\mathbf{a}_2)/2} \sin \frac{\mathbf{k}\cdot\mathbf{a}_3}{2} \\ -e^{i(\mathbf{k}\cdot\mathbf{a}_1 - \mathbf{k}\cdot\mathbf{a}_2)/2} \sin \frac{\mathbf{k}\cdot\mathbf{a}_1}{2} \\ e^{-i(\mathbf{k}\cdot\mathbf{a}_1 - \mathbf{k}\cdot\mathbf{a}_2)/2} \sin \frac{\mathbf{k}\cdot\mathbf{a}_2}{2} \end{pmatrix}, \quad (\text{A5})$$

where $N_1^2 = 4(\sin^2(\mathbf{k} \cdot \mathbf{a}_1/2)) + \sin^2(\mathbf{k} \cdot \mathbf{a}_2/2) + \sin^2(\mathbf{k} \cdot \mathbf{a}_3/2)$.

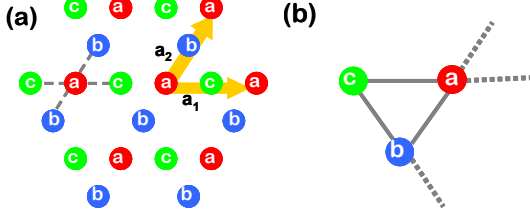


FIG. 6: (a) The Kagome lattice has three atoms per unit cell marked a, b, c . For each atom, we consider the first neighbor hoppings (J_1) shown by the dashed lines. $\mathbf{a}_{1,2}$ are the lattice translation vectors (b) One possible choice of the unit cell. All atoms and bonds wholly belong to the chosen unit cell. The dashed lines are the bonds that extended to the neighboring unit cells and the solid lines are the bonds within this unit cell.

The continuum limit can be obtained by studying the Hamiltonian around the Γ -point. We shall restrict the terms in the Hamiltonian to $\mathcal{O}(k^2)$. This will result in $H_i = 2 - k_i^2$, where $k_i \equiv \mathbf{k} \cdot \mathbf{a}_i$. The resulting characteristic equation is

$$\frac{E}{J_1} \left(\frac{E}{J_1} + 2 \right) \left[\left(\frac{E}{J_1} + 2 \right) \left(\frac{E}{J_1} - 4 \right) + \frac{3}{2} \mathbf{k}^2 \right] = 0. \quad (\text{A6})$$

It can be shown that $E = 0$ is not non-trivial solution. The eigenvalues are thus $E_1 = -2J_1$, $E_{2/3} = J_1 \left(1 \mp 3\sqrt{1 - \mathbf{k}^2/6} \right)$. And the flat band wavefunction [up to $\mathcal{O}(k^2)$] is

$$\Psi_{\mathbf{k}}^1 = \sqrt{\frac{2}{3\mathbf{k}^2}} \begin{pmatrix} k_3 \\ -k_1 \\ k_2 \end{pmatrix} = \sqrt{\frac{2}{3}} \begin{pmatrix} \cos(\theta_{\mathbf{k}} + \frac{\pi}{3}) \\ \cos(\theta_{\mathbf{k}} + \pi) \\ \cos(\theta_{\mathbf{k}} - \frac{\pi}{3}) \end{pmatrix}. \quad (\text{A7})$$

Note that the flat band wavefunction has the property that a rotation of $\pi/3$ causes the weights on the sub lattice to rotate as $a \rightarrow b \rightarrow c \rightarrow a$ and causes the wavefunction to acquire a phase of π . The Kagome lattice is invariant under $a \rightarrow b \rightarrow c \rightarrow a$, but the wavefunction acquires a negative sign under a C_6 rotation. Thus the fermionic ground state possesses an f -wave symmetry. This property is also obeyed by the localized state discussed in Ref. 30. Since this property is maintained by any \mathbf{k} -state, it suggests that any fermionic state with a filling fraction $\nu < 1/3$ also has this character.

1. Real space wavefunctions

The Bloch solution, allows us to write down the solution in real space as

$$\begin{aligned} \psi_{\mathbf{k}}^a(\mathbf{r}) &= \hat{k}_3 \phi_{\mathbf{k}}(\mathbf{r}), \\ \psi_{\mathbf{k}}^b(\mathbf{r}) &= -\hat{k}_1 \phi_{\mathbf{k}}(\mathbf{r}), \\ \psi_{\mathbf{k}}^c(\mathbf{r}) &= \hat{k}_2 \phi_{\mathbf{k}}(\mathbf{r}), \end{aligned} \quad (\text{A8})$$

where $\hat{k}_i \equiv -i\mathbf{a}_i \cdot \partial_{\mathbf{r}}$, and $\phi_{\mathbf{k}}(\mathbf{r})$ is a function that solves the characteristic equation of the Kagome Hamiltonian. Because of the structure of Eq. (A6), we see that $\phi_{\mathbf{k}}(\mathbf{r}) = e^{i\mathbf{k} \cdot \mathbf{r}}$.

Appendix B: The Chern-Simons flux and the covariant momentum

As introduced in the main text, our MFA introduces two fluxes ϕ_C and ϕ_T (which are eventually set equal). While ϕ_C is simply imposed onto the model, ϕ_T originates from a vector potential $\mathbf{A}(\mathbf{r})$ and grows with area (Maxwell-type). We remind the reader that $\mathbf{A}(\mathbf{r})$ is the one that is to be used in creating the covariant momentum $\mathbf{p} = -i\partial_{\mathbf{r}} + \mathbf{A}(\mathbf{r})$. The corresponding translation operators have the following properties:

$$\begin{aligned} p_1 &= p_2 + p_3, \\ e^{-ip_2} e^{-ip_3} e^{ip_1} &= e^{-i\phi_T} = e^{-ip_1} e^{ip_2} e^{ip_3}, \\ e^{-ip_3} e^{-ip_2} e^{ip_1} &= e^{i\phi_T} = e^{-ip_1} e^{ip_3} e^{ip_2}, \\ e^{-ip_3} e^{ip_1} e^{ip_3} e^{-ip_1} &= e^{-2i\phi_T}, \\ e^{-2ip_3} e^{2ip_1} e^{2ip_3} e^{-2ip_1} &= e^{-8i\phi_T} \text{ (area of unit cell)}, \\ e^{ip_3} e^{ip_1} e^{ip_2} &= e^{3i\phi_T} e^{2ip_1}, \\ e^{ip_2} e^{ip_1} e^{ip_3} &= e^{-3i\phi_T} e^{2ip_1}, \\ e^{ip_3} e^{ip_1} e^{ip_2} e^{-ip_3} e^{-ip_1} e^{-ip_2} &= e^{6i\phi_T} \text{ (area of the hexagon)}. \end{aligned}$$

Here $p_i = \mathbf{p} \cdot \mathbf{a}_i$. We further have the following commutation relations for $i, j \in \{1, 2, 3\}$:

$$\begin{aligned} [k_i, k_j] &= 0, \\ [p_1, p_2] &= -2i\phi_T, \\ [p_2, p_3] &= 2i\phi_T, \\ [p_3, p_1] &= -2i\phi_T, \end{aligned} \quad (\text{B1})$$

The flux ϕ_C is introduced to account for the internal modulation and is incorporated directly in the Hamiltonian as shown in Eq (9) of the main text. This is necessary because the continuum limit is obtained from the Bloch solution. The flux ϕ_C , a property of the unit cell itself, cannot be accounted for by introducing a position dependent gauge field like $\mathbf{A}(\mathbf{r})$.

The translational operator on a lattice taking a fermion from \mathbf{r}_1 to \mathbf{r}_2 is $T_{\mathbf{r}_2\mathbf{r}_1} \equiv c_{\mathbf{r}_2}^\dagger c_{\mathbf{r}_1}$. For a triangular loop $L_T : a \rightarrow b \rightarrow c$, it follows that $T(L_T) \equiv T_{\mathbf{r}_a\mathbf{r}_c} T_{\mathbf{r}_c\mathbf{r}_b} T_{\mathbf{r}_b\mathbf{r}_a}$ is the same as $T(L'_T) \equiv T_{\mathbf{r}_a\mathbf{r}_b} T_{\mathbf{r}_b\mathbf{r}_c} T_{\mathbf{r}_c\mathbf{r}_a}$. If we couple the fermions to a Maxwell-type gauge field where the flux grows with the area, then $T_{\mathbf{r}_2\mathbf{r}_1} \rightarrow e^{i\Lambda_{\mathbf{r}_2\mathbf{r}_1}^M} c_{\mathbf{r}_2}^\dagger c_{\mathbf{r}_1}$ and

$$\begin{aligned} T^M(L_T) &= e^{i\phi_T} T(L_T) \\ T^M(L'_T) &= e^{-i\phi_T} T(L_T) \\ \phi_T &= \Lambda_{\mathbf{r}_a\mathbf{r}_c}^M + \Lambda_{\mathbf{r}_c\mathbf{r}_b}^M + \Lambda_{\mathbf{r}_b\mathbf{r}_a}^M = \int \mathbf{A} \cdot d\mathbf{l}. \end{aligned} \quad (\text{B2})$$

Similarly, we may consider the hexagonal loop which yields $T^M(L_H) = e^{i6\phi_T} T(L_H)$.

On implementing the CS flux as shown in Figs. 2c and 3 of the main text, we see that

$$\begin{aligned} T^{CS}(L_T) &= e^{i(\phi_T - \phi_C)} T(L_T) = T(L_T), \\ T^{CS}(L_H) &= e^{i(6\phi_T + 2\phi_C)} T(L_T) = e^{8i\phi_T} T(L_T). \end{aligned} \quad (\text{B3})$$

The last equality is obtained by setting $\phi_T = \phi_C$. Equating the total flux through the unit cell $8\phi_T$ to $6\pi\nu$, we arrive at the relation

$$\phi_T = \phi_C = 3\pi\nu/4. \quad (\text{B4})$$

Appendix C: The flat band wavefunction in a Kagome lattice with CS flux

Before deriving the case with the CS flux, we explicitly derive Eq. (A8). This is informative and the derivation with the CS flux follows similar lines. Plugging the flat band eigenvalue to the Hamiltonian we see that the flat band wavefunction components ψ^a satisfy

$$\begin{aligned} k_2(k_2\psi^a - k_3\psi^c) &= 0, \\ k_3(k_3\psi^b + k_1\psi^a) &= 0, \\ k_1(k_1\psi^c + k_2\psi^b) &= 0. \end{aligned} \quad (\text{C1})$$

It is useful note that other equations can be generated using $a \rightarrow b \rightarrow c \rightarrow a$; $\{H_1, H_1^*\} \rightarrow \{H_2^*, H_2\}$; $\{H_2, H_2^*\} \rightarrow \{H_3, H_3^*\}$; $\{H_3, H_3^*\} \rightarrow \{H_1^*, H_1\}$; and $k_1 \rightarrow k_2$, $k_2 \rightarrow -k_3$, $k_3 \rightarrow k_1$. This implies that $k_1(\psi^a + \psi^b + \psi^c) = \text{const}$. Since $\mathbf{k} \rightarrow -i\partial_{\mathbf{r}}$, normalizability over the whole space not only requires $\text{const} = 0$, but $\psi^a + \psi^b + \psi^c = 0$. The only combination that satisfies the Hamiltonian is then given by Eq. (A8).

It is sometimes inconvenient to have the components of the wavefunctions expressed as operators. To remedy this the action of the operator $\hat{R}_{\mathbf{r}}$ can be implemented by convoluting with the Greens' function of the operator $R(\mathbf{r} - \mathbf{r}')$. Thus

$$\hat{R}_{\mathbf{r}} f(\mathbf{r}) = \int_{\mathbf{r}'} R(\mathbf{r} - \mathbf{r}') f(\mathbf{r}'). \quad (\text{C2})$$

If $\hat{R}_{\mathbf{r}} = -i\partial_{\mathbf{r}}$, then $R(\mathbf{r} - \mathbf{r}') = -i\partial_{\mathbf{r}}\delta(\mathbf{r} - \mathbf{r}') = i\partial_{\mathbf{r}'}\delta(\mathbf{r} - \mathbf{r}')$.

When a similar analysis is carried out for \hat{H}^{MFA} with the CS flux attached, we end up with Eq. (C1) but with

$\mathbf{k} \rightarrow \mathbf{p} \equiv -i\partial_{\mathbf{r}} + \mathbf{A}(\mathbf{r})$ (only for $\phi_T = \phi_C$). The cyclic interchange also works the same way with $\mathbf{k} \rightarrow \mathbf{p}$, and with an addition of $\phi_C \rightarrow -\phi_C$. Just like before, normalizability will enforce that $\psi^a + \psi^b + \psi^c = 0$. This result is independent of the choice of gauge for writing down $\mathbf{A}(\mathbf{r})$. Thus the flat band wavefunction can be written as

$$\begin{aligned} \psi_{\mathbf{k}}^a(\mathbf{r}) &= \hat{p}_3\phi_i(\mathbf{r}), \\ \psi_{\mathbf{k}}^b(\mathbf{r}) &= -\hat{p}_1\phi_i(\mathbf{r}), \\ \psi_{\mathbf{k}}^c(\mathbf{r}) &= \hat{p}_2\phi_i(\mathbf{r}), \end{aligned} \quad (\text{C3})$$

where i is some index denoting the quantum state (which is no longer the momentum). It is worth noting that when this wavefunction is substituted back into the Hamiltonian equations for $E = -2J_1$, we get

$$\begin{aligned} 0 &= 2\psi^a + H_2 e^{i\phi_C} \psi^b + H_1 \psi^c + \mathcal{O}(p^3) \\ &= 2p_3 + (2 - p_2^2)(1 + i\phi_C)(-p_1) + (2 - p_1^2)p_2 + \mathcal{O}(p^3) \\ &= 2(p_3 + p_2 - p_1) - 2ip_1\phi_C + p_2^2 p_1 - p_1^2 p_2 + \mathcal{O}(p^3) \\ &= -2ip_1(\phi_C - \phi_T) + \mathcal{O}(p^3) \\ &= 0 + \mathcal{O}(p^3). \end{aligned} \quad (\text{C4})$$

Note that since our equations are derived correct to $\mathcal{O}(p^2)$, we conclude that the wavefunction guess in Eq. (C3) is correct to $\mathcal{O}(p^2)$.

Appendix D: Normalization of the flat band wavefunction

We require $\int_{\mathbf{r}} \Psi^\dagger(\mathbf{r})\Psi(\mathbf{r}) = 1$. From Eq. (12) of the main text and using the form of $f(\mathbf{r})$, we see that

$$\begin{aligned} \mathcal{N}^2 &= \int_{\mathbf{r}} \left[\sum_i \{p_i^* f(\mathbf{r})\} \{p_i f(\mathbf{r})\} \right] \\ &= \int_{\mathbf{r}} \left[\sum_i \{k_i f(\mathbf{r})\}^2 + \{A_i f(\mathbf{r})\}^2 \right] \\ &= \frac{3}{2} \int_{\mathbf{r}} [\{\partial_x f(\mathbf{r})\}^2 + \{\partial_y f(\mathbf{r})\}^2 + A^2 f^2(\mathbf{r})] \\ &= \frac{3}{4} [1 + gB^2 l_{CS}^4], \end{aligned} \quad (\text{D1})$$

where g is a gauge dependent constant factor. If \mathbf{A} is chosen in Landau gauge, $g = 1/2$. If \mathbf{A} is chosen in symmetric gauge, $g = 1/4$.

¹ T.-H. Han, J. S. Helton, S. Chu, D. G. Nocera, J. A. Rodriguez-Rivera, C. Broholm, and Y. S. Lee, Nature **492**, 406 EP (2012), URL <http://dx.doi.org/10.1038/nature11659>.

² M. Punk, D. Chowdhury, and S. Sachdev, Nature Physics **10**, 289 EP (2014), URL

<http://dx.doi.org/10.1038/nphys2887>.

³ Y. Ran, M. Hermele, P. A. Lee, and X.-G. Wen, Phys. Rev. Lett. **98**, 117205 (2007), URL <https://link.aps.org/doi/10.1103/PhysRevLett.98.117205>.

⁴ Y. Iqbal, F. Becca, and D. Poilblanc, Phys. Rev. B **84**, 020407 (2011), URL

- <https://link.aps.org/doi/10.1103/PhysRevB.84.020407>.
- ⁵ S. Yan, D. A. Huse, and S. R. White, *Science* **332**, 1173 (2011), ISSN 0036-8075, URL <http://science.sciencemag.org/content/332/6034/1173>.
 - ⁶ K. Yang, L. K. Warman, and S. M. Girvin, *Phys. Rev. Lett.* **70**, 2641 (1993), URL <https://link.aps.org/doi/10.1103/PhysRevLett.70.2641>.
 - ⁷ L. Messio, B. Bernu, and C. Lhuillier, *Phys. Rev. Lett.* **108**, 207204 (2012), URL <https://link.aps.org/doi/10.1103/PhysRevLett.108.207204>.
 - ⁸ Y.-C. He, D. N. Sheng, and Y. Chen, *Phys. Rev. Lett.* **112**, 137202 (2014), URL <https://link.aps.org/doi/10.1103/PhysRevLett.112.137202>.
 - ⁹ S.-S. Gong, W. Zhu, and D. N. Sheng, *Scientific Reports* **4**, 6317 EP (2014), article, URL <http://dx.doi.org/10.1038/srep06317>.
 - ¹⁰ B. Bauer, L. Cincio, B. P. Keller, M. Dolfi, G. Vidal, S. Trebst, and A. W. W. Ludwig, *Nature Communications* **5**, 5137 EP (2014), article, URL <http://dx.doi.org/10.1038/ncomms6137>.
 - ¹¹ K. Kumar, K. Sun, and E. Fradkin, *Phys. Rev. B* **90**, 174409 (2014), URL <https://link.aps.org/doi/10.1103/PhysRevB.90.174409>.
 - ¹² K. Kumar, K. Sun, and E. Fradkin, *Phys. Rev. B* **92**, 094433 (2015), URL <https://link.aps.org/doi/10.1103/PhysRevB.92.094433>.
 - ¹³ M. P. Zaletel, Z. Zhu, Y.-M. Lu, A. Vishwanath, and S. R. White, *Phys. Rev. Lett.* **116**, 197203 (2016), URL <https://link.aps.org/doi/10.1103/PhysRevLett.116.197203>.
 - ¹⁴ R. G. Pereira and S. Bieri, *SciPost Phys.* **4**, 004 (2018), URL <https://scipost.org/10.21468/SciPostPhys.4.1.004>.
 - ¹⁵ V. Kalmeyer and R. B. Laughlin, *Phys. Rev. Lett.* **59**, 2095 (1987), URL <https://link.aps.org/doi/10.1103/PhysRevLett.59.2095>.
 - ¹⁶ X. G. Wen, F. Wilczek, and A. Zee, *Phys. Rev. B* **39**, 11413 (1989), URL <https://link.aps.org/doi/10.1103/PhysRevB.39.11413>.
 - ¹⁷ D. V. Khveshchenko and P. B. Wiegmann, *Modern Physics Letters B* **03**, 1383 (1989), URL <https://doi.org/10.1142/S0217984989002089>.
 - ¹⁸ D. V. Khveshchenko and P. B. Wiegmann, *Modern Physics Letters B* **04**, 17 (1990), URL <https://doi.org/10.1142/S0217984990000040>.
 - ¹⁹ A. Kitaev, *Annals of Physics* **321**, 2 (2006), ISSN 0003-4916, january Special Issue, URL <http://www.sciencedirect.com/science/article/pii/S0003491605002384>.
 - ²⁰ H. Yao and S. A. Kivelson, *Phys. Rev. Lett.* **99**, 247203 (2007), URL <https://link.aps.org/doi/10.1103/PhysRevLett.99.247203>.
 - ²¹ C. Xu and S. Sachdev, *Phys. Rev. B* **79**, 064405 (2009), URL <https://link.aps.org/doi/10.1103/PhysRevB.79.064405>.
 - ²² A. Wietek and A. M. Läuchli, *Phys. Rev. B* **95**, 035141 (2017), URL <https://link.aps.org/doi/10.1103/PhysRevB.95.035141>.
 - ²³ Y. Werman, S. Chatterjee, S. C. Morampudi, and E. Berg, *Phys. Rev. X* **8**, 031064 (2018), URL <https://link.aps.org/doi/10.1103/PhysRevX.8.031064>.
 - ²⁴ L. Balents, *Nature* **464**, 199 EP (2010), URL <http://dx.doi.org/10.1038/nature08917>.
 - ²⁵ L. Savary and L. Balents, *Reports on Progress in Physics* **80**, 016502 (2017), URL <http://stacks.iop.org/0034-4885/80/i=1/a=016502>.
 - ²⁶ Y. Zhou, K. Kanoda, and T.-K. Ng, *Rev. Mod. Phys.* **89**, 025003 (2017), URL <https://link.aps.org/doi/10.1103/RevModPhys.89.025003>.
 - ²⁷ O. Benton, L. D. C. Jaubert, R. R. P. Singh, J. Oitmaa, and N. Shannon, *Phys. Rev. Lett.* **121**, 067201 (2018), URL <https://link.aps.org/doi/10.1103/PhysRevLett.121.067201>.
 - ²⁸ M. R. Norman, *Rev. Mod. Phys.* **88**, 041002 (2016), URL <https://link.aps.org/doi/10.1103/RevModPhys.88.041002>.
 - ²⁹ R. Pohle, H. Yan, and N. Shannon, arXiv (2017), URL <https://arxiv.org/abs/1711.03778>.
 - ³⁰ D. L. Bergman, C. Wu, and L. Balents, *Phys. Rev. B* **78**, 125104 (2008), URL <https://link.aps.org/doi/10.1103/PhysRevB.78.125104>.
 - ³¹ S. D. Huber and E. Altman, *Phys. Rev. B* **82**, 184502 (2010), URL <https://link.aps.org/doi/10.1103/PhysRevB.82.184502>.
 - ³² J. K. Jain, *Phys. Rev. Lett.* **63**, 199 (1989), URL <https://link.aps.org/doi/10.1103/PhysRevLett.63.199>.
 - ³³ A. Lopez and E. Fradkin, *Phys. Rev. B* **44**, 5246 (1991), URL <https://link.aps.org/doi/10.1103/PhysRevB.44.5246>.
 - ³⁴ B. I. Halperin, P. A. Lee, and N. Read, *Phys. Rev. B* **47**, 7312 (1993), URL <https://link.aps.org/doi/10.1103/PhysRevB.47.7312>.
 - ³⁵ S. C. Zhang, T. H. Hansson, and S. Kivelson, *Phys. Rev. Lett.* **62**, 82 (1989), URL <https://link.aps.org/doi/10.1103/PhysRevLett.62.82>.
 - ³⁶ T. A. Sedrakyan, A. Kamenev, and L. I. Glazman, *Phys. Rev. A* **86**, 063639 (2012), URL <https://link.aps.org/doi/10.1103/PhysRevA.86.063639>.
 - ³⁷ T. A. Sedrakyan, V. M. Galitski, and A. Kamenev, *Phys. Rev. Lett.* **115**, 195301 (2015), URL <https://link.aps.org/doi/10.1103/PhysRevLett.115.195301>.
 - ³⁸ T. A. Sedrakyan, L. I. Glazman, and A. Kamenev, *Phys. Rev. B* **89**, 201112 (2014), URL <https://link.aps.org/doi/10.1103/PhysRevB.89.201112>.
 - ³⁹ T. A. Sedrakyan, V. M. Galitski, and A. Kamenev, *Phys. Rev. B* **95**, 094511 (2017), URL <https://link.aps.org/doi/10.1103/PhysRevB.95.094511>.
 - ⁴⁰ R. Wang, B. Wang, and T. A. Sedrakyan, *Phys. Rev. B* **98**, 064402 (2018), URL <https://link.aps.org/doi/10.1103/PhysRevB.98.064402>.
 - ⁴¹ R. Wang, T. A. Sedrakyan, B. Wang, and D. Xing (2017), URL <https://arxiv.org/abs/1712.06762>.
 - ⁴² T. A. Sedrakyan, L. I. Glazman, and A. Kamenev, *Phys. Rev. Lett.* **114**, 037203 (2015), URL <https://link.aps.org/doi/10.1103/PhysRevLett.114.037203>.
 - ⁴³ R. Sohal, L. H. Santos, and E. Fradkin, *Phys. Rev. B* **97**, 125131 (2018), URL <https://link.aps.org/doi/10.1103/PhysRevB.97.125131>.
 - ⁴⁴ S. Bieri, L. Messio, B. Bernu, and C. Lhuillier, *Phys. Rev. B* **92**, 060407 (2015), URL <https://link.aps.org/doi/10.1103/PhysRevB.92.060407>.
 - ⁴⁵ S. Bieri, C. Lhuillier, and L. Messio, *Phys. Rev. B* **93**, 094437 (2016), URL <https://link.aps.org/doi/10.1103/PhysRevB.93.094437>.
 - ⁴⁶ S. Maiti and T. A. Sedrakyan, arXiv **1812.10153** (2019), URL <https://arxiv.org/abs/1812.10153>.
 - ⁴⁷ Y.-M. Lu and A. Vishwanath, *Phys. Rev. B* **86**, 125119 (2012), URL <https://link.aps.org/doi/10.1103/PhysRevB.86.125119>.
 - ⁴⁸ X.-G. Wen, *Advances in Physics* **44**, 405 (1995), URL <https://doi.org/10.1080/00018739500101566>, URL

- <https://doi.org/10.1080/00018739500101566>.
- ⁴⁹ G.-B. Jo, J. Guzman, C. K. Thomas, P. Hosur, A. Vishwanath, and D. M. Stamper-Kurn, Phys. Rev. Lett. **108**, 045305 (2012), URL <https://link.aps.org/doi/10.1103/PhysRevLett.108.045305>.
- ⁵⁰ M. Atala, M. Aidelsburger, M. Lohse, J. T. Barreiro, B. Paredes, and I. Bloch, Nature Physics **10**, 588 EP (2014), article, URL <http://dx.doi.org/10.1038/nphys2998>.
- ⁵¹ J. Stenger, S. Inouye, A. P. Chikkatur, D. M. Stamper-Kurn, D. E. Pritchard, and W. Ketterle, Phys. Rev. Lett. **82**, 4569 (1999), URL <https://link.aps.org/doi/10.1103/PhysRevLett.82.4569>.
- ⁵² A. M. Rey, P. B. Blakie, G. Pupillo, C. J. Williams, and C. W. Clark, Phys. Rev. A **72**, 023407 (2005), URL <https://link.aps.org/doi/10.1103/PhysRevA.72.023407>.
- ⁵³ P. T. Ernst, S. Götze, J. S. Krauser, K. Pyka, D.-S. Lühmann, D. Pfannkuche, and K. Sengstock, Nature Physics **6**, 56 EP (2009), article, URL <http://dx.doi.org/10.1038/nphys1476>.